Chapter 1

Introduction

In this chapter we provide a broad overview of GWs including the formalisms that provide the basic inputs for the calculations presented in this thesis. This biased and incomplete overview is based very heavily on many review articles. In particular Section 1.1 on [1], Section 1.2 on [2], Section 1.3 on [3, 1], Section 1.4 on [1, 2], Sections 1.5-1.6 on [4], Sections 1.8-1.9 on [5, 6], Sections 1.12-1.17 on [7], Section 1.20 on [8], and finally Section 1.21 on [9].

1.1 What are gravitational waves?

General relativity (GR) and electrodynamics display deep and profound similarities and yet there exist fundamental differences between them. Let us take a look at some of the historical similarities between the two fields.

Maxwell's equations together with the Lorentz force equation successfully incorporate all the laws of electricity and magnetism. Using them, Maxwell was able to predict the existence of a solution consisting of electric and magnetic fields changing with time. This solution transfers energy and propagates with speed c in vacuum. These are electromagnetic waves (EMW). Distinguished physicists, such as Lord Kelvin, had serious doubts about the existence of such waves. However, in just eight years after Maxwell's death, Heinrich Hertz generated and detected electromagnetic waves in the laboratory. In 1901 electromagnetic signals were transmitted and received across the Atlantic Ocean.

Our view of the universe comes from the EMWs observed from it. Radio waves revealed for instance, quasars, jets from galactic nuclei, rapidly rotating pulsars and cosmic microwave background, the relic of the hot big bang. X-rays revealed accretion disks about neutron stars (NS) and black holes (BH). Infrared and ultraviolet observations and gamma ray burst observations have opened new windows to the universe going beyond conventional optical astronomy.

Einstein's field equations of general relativity describe the gravitational interaction via the space-time curvature generated by mass-energy. General relativity is a theory of gravity that is consistent with special relativity. In particular, with the principle that nothing travels faster than light. This means that the gravitational field must propagate with speed not larger than ***c***. On the basis of his field equations Albert Einstein showed that the changes (curvature perturbations) propagate at exactly the same speed as vacuum electromagnetic waves, "the speed of light ***c***". These propagating changes are called gravitational waves.

General relativity is a nonlinear theory and there is, in general, no sharp distinction between the part of the metric that represents the waves and the rest of the metric. Only in certain approximations can we clearly define gravitational radiation. They include:

- Linearized theory: It is a weak-field approximation to general relativity (first used by Einstein), where the equations are written and solved in a nearly flat space-time. The static and wave parts of the field cleanly separate. Gravitational waves are idealized as a 'ripple' propagating through a flat and empty universe. This picture is a simple case of the more general 'short-wave approximation', in which waves appear as small perturbations of a smooth background that is time dependent and whose radius of curvature is much larger than the wavelength of the waves.

- Perturbation theory: This is a generalization of linearized theory which studies linear perturbations but about a given smooth, time-independent background metric. By studying the tensor perturbations in Schwarzschild and Kerr spacetimes one can compute GWs to very high accuracy.

Einstein's treatment of gravitational wave theory was based on a linearized theory treating weak waves as weak perturbations of a flat background. Similar to what happened in the case of EMWs many physicists had serious doubt about their existence. The linearized theory of GWs had its limits because the linear approximation is not valid for sources where gravitational self- energy is not negligible. In 1941 Landau and Lishitz analysed the emission of GWs by a self-gravitating system of slowly moving bodies and showed that at leading order, Einstein's quadrupole formula was indeed correct. A mathematically rigorous treatment of asymptotics using global methods in GR was necessary to show that GW indeed carry energy. The strongest evidence for the existence of GWs comes from the observation of the energy loss from the binary pulsar system PSR 1913+16, discovered in 1974 by Hulse and Taylor. Though impressive, the evidence is ***indirect*** and one would like to accomplish a ***direct*** detection of GWs on the earth. This is why today GWs, both theory and experiment, is one of the main topics of research in general relativity and gravitation. The detection of GWs will eventually lead to GW Astronomy which in turn is expected to bring a revolution in our knowledge of the universe.

1.2 Why study gravitational waves?

Gravitational radiation is today one of the last unopened windows into the Universe. There are many reasons motivating scientists to work towards gravitational wave astronomy. The main reasons are:

- Gravitational waves arrive unaffected by any intervening matter and carry uncorrupted information even if they come from the most distant parts or most hidden regions of the Universe.
- Since the gravitational waves are emitted by the bulk motions of massive sources and not by individual atoms or electrons as in the case of electromagnetic waves, they carry a completely different kind of information about their sources.
- Gravitational waves provide the only way to make ***direct*** observations of black holes. Since there is now strong indirect evidence that giant black holes inhabit the centers of many (or even most) galaxies, and since smaller ones are common in the Galaxy, there is great interest in making direct observations of them.
- Gravitational waves can come from extraordinarily early epochs in the history of the Universe. Observations of the cosmic microwave background, the electromagnetic relic radiation from the big bang, describes the Universe as it was at about 10^5 years after the Big Bang. If a cosmological background of gravitational waves is detected it would provide a picture of the Universe much earlier on, just at the end of inflation (about 10^{-24} seconds old).
- Gravitational radiation is the last fundamental prediction of Einstein's general relativity that has not yet been ***directly*** verified.

1.3 Linearized theory

The metric in special relativity is[1]

$$ds^2 = \eta_{ab} dx^a dx^b \,, \tag{1.1}$$

where η_{ab} denotes the matrix $\mathrm{diag}(-1, 1, 1, 1)$. Linearized gravity is an adequate approximation to general relativity when the spacetime metric, g_{ab}, may be treated as deviating only

[1] We choose units in which c = G = 1; a, b, c, ... h indices run from 0 lo 3 and i, j, k, ... n indices run from 1 to 3. Repeated indices are summed. The metric has positive signature.

slightly from a flat metric, η_{ab}:

$$gab = \eta_{ab} + h_{ab}, \qquad \|h_{ab}\| \ll 1 \ . \tag{1.2}$$

Here $\|h_{ab}\|$ means "the magnitude of a typical non-zero component of h_{ab}". The condition $\|h_{ab}\| \ll 1$ needs both the gravitational field to be weak, and in addition constrains the coordinate system to be approximately Cartesian. In linearized gravity, the smallness of the deviation means that we only keep terms which are linear in h_{ab} — higher order terms are discarded. As a consequence, indices are raised and lowered using the flat metric η_{ab}. The metric perturbation h_{ab} transforms as a tensor under Lorentz transformations, but not under general coordinate transformations. In the Lorentz gauge $\partial_a h^{ab} = 0$, Einstein's equations reduce to:

$$G_{ab} = -\frac{1}{2}\Box\bar{h}_{ab} \ . \tag{1.3}$$

The linearized Einstein equation is therefore

$$\Box\bar{h}_{ab} = -16\,\pi\,T_{ab} \ ; \tag{1.4}$$

which in vacuum, reduces to

$$\Box\bar{h}_{ab} = 0 \ . \tag{1.5}$$

Just as in electromagnetism, the equation (1.4) admits a class of homogeneous solutions which are superpositions of plane waves:

$$\bar{h}_{ab}(\mathbf{x}, t) = \mathrm{Re}\int d^3k\, A_{ab}(\mathbf{k}) e^{i(\mathbf{k}\cdot\mathbf{x}-\omega t)} \ . \tag{1.6}$$

Here, w = $|\mathbf{k}|$. The complex coefficients $A_{ab}(\mathbf{k})$ depend on the wavevector k but are independent of x and ***t***. They are subject to the constraint $k^a A_{ab} = 0$ (which follows from the Lorentz gauge condition), with k^a = (w, k), but are otherwise arbitrary. These solutions are gravitational waves.

Linearized theory describes the classical gravitational field by a massless spin 2 field. It thus propagates at the speed of light and is expected to have only two independent degrees of freedom (polarizations in classical terms). To see this, we recall that h_{ab} is symmetric, so it has ten independent components, and that the Lorentz gauge applies four independent conditions to these, reducing the freedom to six. However, the Lorentz gauge does not fully fix the coordinates. In fact if we perform another infinitesimal coordinate transformation (X $\rightarrow$ $x^a + \xi^a$ with $\partial_b\xi^a = O(h)$) and impose $\Box\xi^a = 0$, we remain in Lorentz gauge. We can

use this freedom to demand:

$$\begin{aligned} A_{0a} &= 0 \Rightarrow A^{ij} k_j = 0 \text{ (transverse wave),} \\ A^a_a &= 0 \text{ (traceless wave).} \end{aligned} \tag{1.7}$$

These conditions can only be applied outside a sphere surrounding the source. Together they put the metric into the transverse-traceless (TT) gauge.

Using the TT gauge leaves only two independent polarizations out of the original ten, and it ensures that $\bar{h}_{ab} = h_{ab}$. In order to understand the polarization degrees of freedom, let us lake the wave to be moving in the z-direction, so that $k_z = w$, $\mathbf{k}^0 = w$, $k_x = 0$, $k_y = 0$. The TT gauge conditions in equations Eq. (1.7) lead to $A_{0a} = \mathbf{A}$, $= 0$ and $\mathbf{A}$, $= -\mathbf{A}$,,. This leaves only two independent components of the polarization tensor, $\mathbf{A}$, and $\mathbf{A}$,.

$\mathbf{A}$ wave for which $A_{xy} = 0$ produces a metric of the form:

$$ds^2 = -dt^2 + (1 + h_+)dx^2 + (1 - h_-)dy^2 + dz^2 , \tag{1.8}$$

where $h^{TT}_{xx} = -h^{TT}_{yy} = h_+$ Such a metric produces opposite effects on proper distance along the two transverse axes, contracting one while expanding the other.

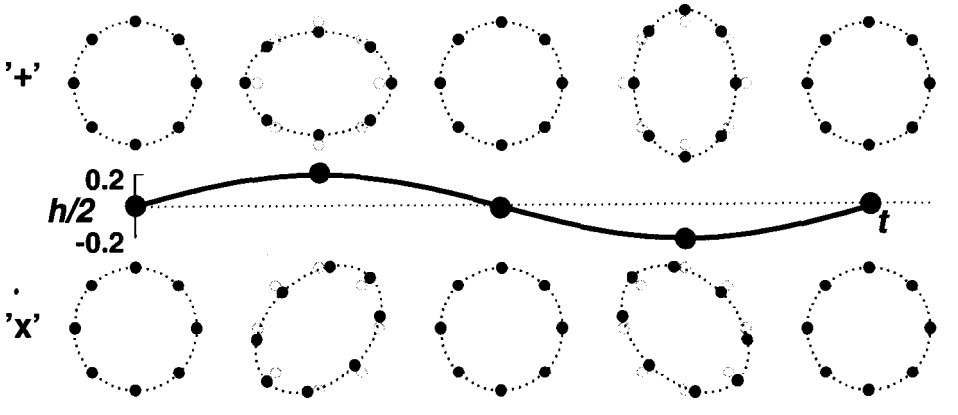

Figure 1.1: Two independent polarisations of a plane gravitational wave are illustrated by their actions on a ring of free particles in empty space. The waves act transversely, so in this figure the waves approach perpendicular to the paper. The waves distort the ring into ellipses with alternating major and minor axes [2].

If $A_{xx} = 0$ we have pure cross polarization $h_x = h_{xy}^{TT} = h_{yx}^{TT}$ which can be obtained from the previous case by a simple 45 rotation (See Fig. [1.1]).

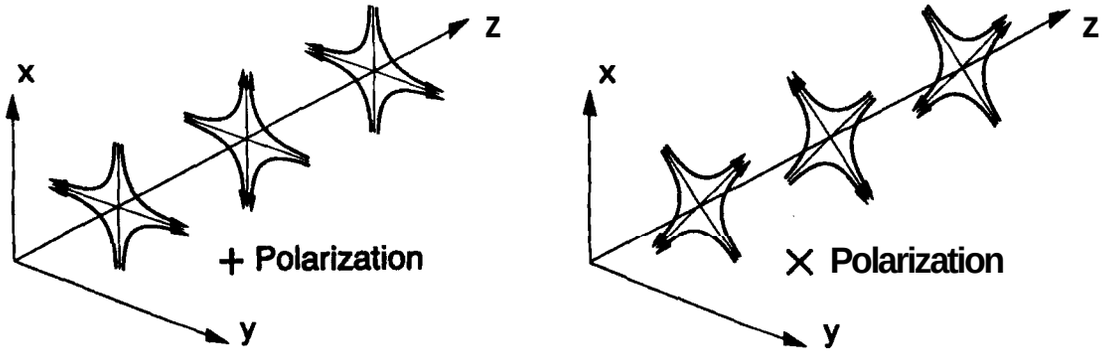

Figure 1.2: The lines of force associated with the two polarizations of a gravitational wave. (From Ref. [10].)

1.4 Effect of a gravitational wave on a system of particles

Tidal forces show the action of the gravitational wave independently of the coordinates. Let us consider the equation of geodesic deviation, which governs the separation of two neighbouring freely-falling test particles **A** and B. If the particle is initially at rest, then as the wave passes it produces an oscillating curvature tensor, and the separation ξ of the two particles is:

$$\frac{d^2\xi^i}{dt^2} = R^i{}_{0j0}\,\xi^j \tag{1.9}$$

To calculate the component R^i_{0j0} of the Riemann tensor in Eq. (1.9), we can use the metric in the TT gauge, because the Riemann tensor is gauge-invariant at linear order. Therefore, we can replace R^i_{0j0} by

$$R^i_{0j0} = \frac{1}{2}\partial_{00}\,h^{TT\,i}{}_{j}\,, \tag{1.10}$$

and write

$$\frac{d^2\xi^i}{dt^2} = \frac{1}{2}\partial_{00}\,h^{TT\,i}{}_{j}\,\xi^j\,. \tag{1.11}$$

This equation, with an initial condition $\xi^j(0)$= constant, describes the oscillations of B's location as measured in the proper reference frame of **A.** The validity of **Eq.** (1.11) is the same as that of the geodesic deviation equation: geodesics have to be close to one another, in a neighbourhood where the change in curvature is small. In this approximation a gravitational

wave is like an extra force, called a tidal force, perturbing the proper distance between two test particles. If there are other forces on the particles, so that they are not free, then as long as the gravitational field is weak, one can just add the tidal forces to the other forces and work as if the particle were in special relativity.

The TT gauge is a special coordinate system in which the polarization tensor of a plane gravitational wave assumes a very simple form. This gauge is comoving for freely-falling particles and so it is not the locally Minkowskian coordinate system that would be used by an experimenter to analyse an experiment. In GR one must always be aware of how one's coordinate system is defined. We shall face two typical situations:

- The detector is small compared to the wavelength of the gravitational waves it is measuring. In this case the geodesic deviation equation Eq. (1.9) represents the wave as a simple extra force on the equipment. Bars detectors can always be analysed in this way. Laser interferometers on the Earth can be treated this way too. In these cases a gravitational wave simply produces a force to be measured.

- The detector is comparable to or larger than that wavelength. Here the geodesic deviation equation is not useful because we have to abandon the 'local 'discussion in terms of the geodesic deviation and use instead a more 'global' treatment in terms of the TT gauge and metric components h^{TT}_{ab}. Space-based interferometers like laser interferometers space antenna (LISA), accurate ranging to solar-system spacecraft and pulsar timing are all in this class.

We conclude this section with an order of magnitude estimate of the effects we are discussing. The amplitude of GWs from a stellar mass source that emits a small fraction of its total mass as GWs over a time scale of a few milliseconds would be

$$h \sim 4\times 10^{-21}\left(\frac{E}{10^{-7}M_\odot}\right)^{1/2}\left(\frac{5\ \text{ms}}{T}\right)^{1/2}\left(\frac{200\ \text{Hz}}{f}\right)\left(\frac{40\ \text{kpc}}{r}\right). \tag{1.12}$$

Thus two masses separated by a distance of $\ell = 1$ km will be tidally distorted by no more than 4×10^{-18} m by such a wave. This leads to a phase change of order 5×10^{-10} radians in an interferometer that uses 0.1 micron laser and whose arms are 4 km long.

1.5 Gravitational wave detectors

1.5.1 Ground-based detectors

There are two types of GW detectors that are currently in operation taking sensitive data:

1. ***Bar detectors:*** Resonant bars operate in a narrow band of 10–50 Hz at a frequency of about 950 Hz. In a bar detector the vibrations induced in a seismically isolated, cryogenic Alumninium or Niobium cylindrical bar is amplified using a transducer. There are currently five such detectors operating around the world, one in Australia (NIOBE), three in Italy (NAUTILUS [11], AURIGA [12], Explorer[2]) and one in the US (ALLEGRO). Bar detectors are limited by background noises caused by internal thermal noise and the quantum uncertainty principle. Current detectors have a strain sensitivity of about $10^{-21}\,\mathrm{Hz}^{-1/2}$ and are mainly sensitive to supernovae in the neighbourhood of the Milky Way and in-band continuous wave sources.

2. *Interferometers:* Interferometers operate in a broad band (1 kHz) at a central frequency of 150 Hz. In a laser interferometric antenna the tidal deformation caused in the two arms of a Michelson interferometer is sensed as a shift in the fringe pattern at the output port of the interferometer. The sensitivity of such a detector is limited at low frequencies (10–40 Hz) by ***seismic disturbances and noises caused by human activities,*** at intermediate frequencies (40–300 Hz) by ***thermal noise of optical and suspended components,*** and at high frequencies (> 300 Hz) by ***photon shot noise.***

   Three key technologies have made it possible to achieve the current level of sensitivities details of which we do not mention here:

   (a) ***Signal recycling*** is particularly useful for observing long-lived continuous wave sources.

   (b) ***Multiple suspension systems*** that filter the ground motion and keep the mirrors essentially free from seismic disturbances.

   (c) ***Monolithic suspensions*** that help isolate the thermal noise to a narrow frequency band.

   There are currently six long baseline detectors in operation: The American Laser Interferometer Gravitational-Wave Observatory (LIGO) [13], which is a network of three detectors, two with 4 km arms and one with 2 km arms, at two sites (Hanford, Washington and Livingstone, Louisiana), the French-Italian VIRGO detector with 3 km arms at Pisa [14], the British-German GEO 600 [15] with 600 m arms at Hannover

[2] The Explorer detector is operated by an Italian group but located in CERN

and the Japanese TAMA with 100 m arms in Tokyo [16]. Australia has built a 100 m test facility with a plan to build a km-size detector sometime in the future.

Plans are well underway both in Europe and the USA to build, by 2008, the next generation of interferometers that are 10–15 times more sensitive than the initial interferometers. With a peak sensitivity of $h \sim 10^{-24}\,\mathrm{Hz}^{-1/2}$ these advanced detectors will be able to detect NS ellipticities as small as 10^{-6} in our Galaxy, BH-BH binaries at a redshift of $z \sim 0.5$, stochastic background at the level of $\Omega_{\rm GW} \sim 10^{-8}$. An important step towards this is the planned European gravitational observatory (EGO) which is a 3rd generation GW antenna. From the above discussion it should be clear that due to the seismic noise interferometers on the earth will not be able to detect GWs with frequencies below 1 Hz. Many known astrophysical sources radiate in this frequency band and to look for them the only alternative at present is to go to space. We discuss it next.

1.5.2 Space-based interferometers

The Laser Interferometer Space Antenna (LISA) is scheduled to fly in 2015. A joint mission of ESA and NASA, it consists of three spacecraft in heliocentric orbit, 60 degrees behind the Earth, in an equilateral triangular formation of size 5 million km [17]. LISA's sensitivity is limited by difficulties with long time-scale ($< 10^{-4}$ Hz) stability, photon shot-noise ($\sim 10^{-3}$ Hz) and large size ($> 10^{-1}$ Hz). LISA will be able to observe galactic, extra-galactic and cosmological point sources as well as stochastic backgrounds from different astrophysical populations and perhaps from certain primordial processes. In addition to LISA there have been proposals to build an antenna in the frequency gap of LISA and ground-based detectors. The ***Deci-Hertz Interferometer Gravitational-Wave Observatory*** (DECIGO) [18] by the Japanese team and the ***Big-Bang Observer*** (BBO), a possible follow-up of LISA [19], are aimed as instruments to observe the primordial GW background and to answer cosmological questions on the expansion rate of the Universe and dark energy.

Fig. 1.3 shows in solid lines the design sensitivity goals of the ground-based interferometers, Initial LIGO and Advanced LIGO. The inset shows the same for the space-based LISA. Also plotted in Fig. 1.3 are source strengths to be discussed in Sec. 1.6

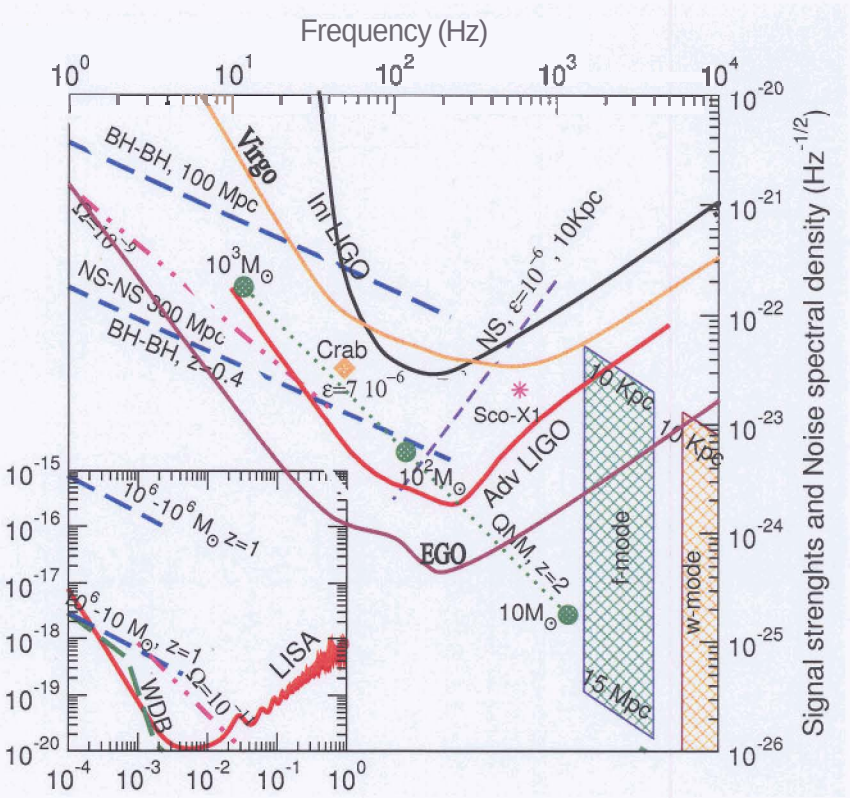

Figure 1.3: Noise PSD (in $Hz^{-1/2}$) **of space-based LISA and four generations of ground-based interferometers,** initial **LIGO, Virgo, advanced** LIGO **and** EGO **respectively.** Also **plotted** on **the** same **graph are *the*** source **strengths for** archetypal **binary, continuous and** stochastic **radiation in the same units. A source will be visible** in **a network** of **4 interferometers** if **it *is* roughly 5** times **above the noise PSD.** This figure **is adapted from** [4]

1.6 Gravitational wave astronomy: Sources and event rates

Gravitational wave detectors could **reveal** hidden **secrets** of the **Universe by helping us to** study **sources in extreme** physical situations: **strong** non-linear **gravity, relativistic** motion, **extremely high density, temperature or magnetic fields. Important among** them **are *compact objects*** (**in isolation** or in **binaries**) and ***stochastic backgrounds.***

1.6.1 Compact binaries

Compact binaries, consisting of a pair of neutron stars or black holes are good standard candles for astronomy [20]. Its chirp mass $\mathrm{M} \equiv \eta^{2/3} M$, completely fixes the absolute luminosity of the system. By observations of the GWs from a binary, we can measure the luminosity distance to the source provided the source chirps, in other words, the orbital frequency changes significantly (as much as $1/T$) during an observational period T. This feature allows one to accurately measure cosmological parameters and their variation as a function of red-shift.

The dynamics of a compact binary consists of three phases:

1. Early inspiral: In this phase, the system spends 100's of millions of years but the power emitted in GW is relatively low. This phase can be treated using linearized Einstein's equations, post-Newtonian theory and energy balance between the binding energy and the emitted radiation. The emitted GW signal is a characteristic chirp waveform with its amplitude and frequency slowly increasing with time. The inspiral phase is calculationally terminated at the last stable orbit (LSO) when the effective potential of the system undergoes a transition from having a well-defined minimum to the one without a minimum. This roughly occurs when the frequency of GW is $f_{\mathrm{LSO}} \simeq 4400\,(M_\odot/M)\,\mathrm{Hz}$. For $\mathrm{M} \lesssim 10 M_\odot$, only the inspiral phase is sensed by the interferometers. The phase evolution of the signal is well modelled during this epoch and matched filtering technique can be used to enhance the visibility of the signal by roughly the square root of the number of signal cycles. Since a large number of cycles are available it is possible to discriminate different signals and accurately measure the parameters of the source such as its location [21], mass and spin [22].

2. Late inspiral, plunge and merger: In this phase the two stars orbit each other at speed $v = c/3$ and experience strong gravitational fields (gravitational potential $\varphi = \mathrm{GM/Rc^2} \sim 0.1$.). This phase requires for its description the full non-linear structure of Einstein's equations as it involves strong relativistic gravity, tidal deformation (in the case of BH-BH or BH-NS) and disruption (in the case of BH-NS and NS-NS). It has been a frontier area of research for numerical relativists [23] for more than two decades. Partial insights have been gained by the application of resurnmation and effective-one-body techniques aimed at accelerating the convergence properties of post-Newtonian expansions of the energy and flux required in constructing the phasing of GW [24, 25, 26]. This is the most interesting phase from the point of view of testing non-linear gravity. Even the total amount of energy radiated during this phase is highly uncertain, with estimates in the range 10% [27] to 0.07% [25]. Since the phase is not well-modelled, it is necessary to employ sub-optimal techniques, such as time-frequency analysis, to detect this phase.

3. ***Late merger:*** This is the phase when the two systems have merged to form either a single NS or a BH, settling down to a quiet state by radiating the deformations induced during the merger. The emitted radiation can be studied using perturbation theory and computing the quasi-normal modes (QNM). The QNMs carry a unique signature that depends only on the mass and spin angular momentum in the case of BH, but depends also on the equation-of-state (EOS) of the material in the case of NS. This should allow one to test whether or not the resultant remanent is a BH or NS. Flanagan and Hughes [27] argue that during the late stages of merger the energy emitted in the form of QNM might be as large as 3% of the system's total mass [27]. The corresponding estimate by Buonanno and Damour is only 0.7% of the system's total mass [25]. Matched filtering, should allow one to detect the QNM resulting from binary mergers of mass in the range $60–10^3\ M_\odot$ at a distance of 200 Mpc in initial LIGO and from $z \sim 2$ in advanced LIGO.

1.6.2 Event rates

1.6.2.1 NS-NS binaries

Double NS can be seen in advanced LIGO to a distance of 300 Mpc (see Fig. 1.3). Based on the observed small population of double NS binaries which merge within the Hubble time Kalogera et al. [28] conclude that the galactic coalescence rate is $\sim 1.8 \times 10^{-4}\ \mathrm{yr}^{-1}$. This implies an event rate of NS-NS coalescences of 0.25 and 1500 yr^{-1}, in initial and advanced LIGO, respectively. An event rate as large as in advanced LIGO and EGO will provide a valuable catalogue to test astronomical paradigms, like for example whether y-ray bursts are associated with NS-NS or NS-BH mergers [29].

1.6.2.2 NS-BH binaries

Advanced interferometers will be sensitive to NS-BH binaries out to a distance of about 650 Mpc. The rate of coalescence of such systems is not known empirically as there have been no astrophysical NS-BH binary identifications. Event rates are derived from population synthesis models which give [30] a galactic coalescence rate in the range $3 \times 10^{-7}–5 \times 10^{-6}\ \mathrm{yr}^{-1}$. The event rate of NS-BH binaries will be worse than that of the BH-BH of the same total mass by a factor of $(4\eta)^{3/2}$ just due to the fact that the SNR scales down as $\sqrt{4\eta}$. Taking these factors into account we get an optimistic detection rate of NS-BH of 1 to 1500 in initial and advanced LIGO, respectively.

1.6.2.3 BH-BH binaries

Black hole mergers are the most promising candidate sources for a first direct detection of GW. The reach of the interferometers for BH-BH binaries varies from 100 Mpc (with the inspiral signal only) to 150 Mpc (inspiral plus merger signal) in initial LIGO, to a red-shift of $z = 0.4$–0.55 in advanced LIGO (cf. Fig. 1.3). As for NS-BH binaries, there is no empirical estimate of the event rate. Population synthesis models are highly uncertain about the galactic rate of BH-BH coalescences and predict [30] a range of 3×10^{-8}–10^{-5} yr^{-1}, smaller than the predicted rate of NS-NS coalescences. Yet, owing to their greater masses, BH-BH event rate in GW detectors is larger than the NS-NS event rate by a factor $M^{5/2}$ for $M \lesssim 100\,M_{\odot}$. The predicted event rate is a maximum of 1 yr^{-1} in initial LIGO and 500 yr^{-1} to 20 day^{-1} in advanced LIGO.

1.6.2.4 Massive black hole binaries

The mergers of MBHs in LISA will be the most spectacular events (see SNR's figures in chapter 5) requiring no templates for signal identification, although good models would be needed to extract source parameters. Mergers can be seen to $z \sim 30$ and, therefore, one could study the merger-history of galaxies throughout the Universe and address astrophysical questions about the origin, growth and population of MBH.

The predicted rate for MBH mergers is the same as the rate at which galaxies merge, about 1 yr^{-1} out to a red-shift of $z = 5$ [31].

1.6.3 Stochastic background

A population of unresolved background sources [30] or quantum processes in the early Universe produce stochastic GW signals. By detecting such a stochastic background one can learn more about the underlying population distribution and operative physical processes in the early universe. A network of antennas can be used to discover stochastic signals buried in the instrumental noise backgrounds since it is expected that the instrumental backgrounds will be different in two geographically well-separated antennas. By cross-correlating the data from two detectors one can eliminate the background and extract the interesting stochastic signal. For non co-located detectors, the SNR builds only over GW wavelengths longer than twice the distance between antennas. For the two LIGO antennas at Lousiana and Hanford this means only over frequencies below about 40 Hz [32].

1.6.3.1 Astronomical backgrounds

There are thousands of white dwarf binaries in our galaxy and their period ranges from a few hours to 100 seconds. Though each binary will emit radiation at a single frequency, over an observation period T each frequency bin of width $\mathbf{Af} = 1/T$ will be populated by many sources. Unless the source is close by it will not be possible to detect it amongst the *confusion* background created by the underlying population.

1.6.3.2 Primordial background

A cosmological GW background can be created in the very early Universe and later amplified via parametric amplification, due to coupling to the background gravitational field [30].

Observing such a background is of fundamental importance as this is the only way we can ever hope to directly witness the birth of the Universe. The cosmic microwave background, being strongly coupled to baryons for 300,000 years after the big bang loses the signature of the early Universe. The GW background, on the other hand, would de-couple from the rest of the matter 10^{-24} s after the big bang, and would carry uncorrupted information about the origin of the Universe. The strength of stochastic GW background is measured in terms of the fraction Ω_{GW} of the energy density in GW as compared to the critical density needed to close the Universe. The amplitude of GW is given by [33]: $h = 8 \times 10^{-19} \Omega_{GW}^{1/2}/f$, for $H_0 = 65$ km s^{-1} Mpc.

In the standard inflationary model of the early Universe, the energy density expected in GW is $\Omega_{GW} \lesssim 10^{-15}$, and this cannot be detected by future ground-based detectors or even LISA. Space missions currently being planned (DECIGO/BBO) to exploit the astrophysically quiet band of 10^{-2}–1 Hz might detect the primordial GW and offer a glimpse to the origin of the Universe.

1.7 Conventions on source strengths and units

Prototypical sources for ground based detectors involve neutron stars (NS) and (stellar mass) black holes (BH) whose masses are assumed to be $M = 1.4M_{\odot}$ (radius R = 10 km) and $M = 10M_{\odot}$ respectively. While speaking of the detectability of a source, one assumes that a broadband source of known phase evolution is integrated over a bandwidth equal to its frequency, for continuous waves an integration time of 10^7 s, for stochastic signals an integration over 10^7 s over a bandwidth $\mathbf{f}$, and for quasi-normal modes an integration over one e-folding time. With this choice, the raw dimensionless amplitude of GW is re-expressed in units of $\mathrm{Hz}^{-1/2}$, allowing one to compare source strengths with the antenna's amplitude noise spectral density $\sqrt{S_h(f)}$, which is also measured in units of $\mathrm{Hz}^{-1/2}$. For a 1% false alarm

probability during the course of observation it is typically necessary to set signal-to-noise ratio (SNR) threshold of about 8 in a single detector. In a network consisting of three equally sensitive detectors, in order that the network-SNR is 8, each instrument must register an SNR of ~ 5. Thus a source is considered observable if the SNR it produces is at least 5. The SNR achievable for point sources indeed depends on the orientation of the source relative to the detector. One assumes that sources occur with random orientations and considers the typical source to have an "RMS" orientation. The amplitude of a source with an "RMS" orientation is smaller than an optimally oriented source by a factor of $5/2$ [34].

1.8 Matched filtering

As seen from the discussions in the earlier sections, the weakness of gravity implies GWs are extremely weak. There can be no laboratory sources and one needs to look for astrophysical GWs like chirps from inspiralling compact binaries, bursts from supernova or gamma-ray bursts, monochromatic periodic sources like pulsars or stochastic background of GWs from unresolved populations or the early universe. Even strong sources like NS-NS, BH-BH or supernovae represent weak signals buried in noise of terrestrial detectors like LIGO and VIRGO. One must use a technique like matched filtering to detect the wave and extract its parameters. We briefly summarise the main features of matched filtering next.

A matched filter compares two signals and outputs a function describing the values at which the two signals are most like one another. The comparison is via correlation. Correlation superposes one function over another function and produces a single value characterising a level of similarity. It then moves the first function an infinitesimally amount and recomputes another value. The final result is a graph which peaks at the point where the two images are most similar. correlation in the time domain (the domain in which we would want to compare two signals) just happens to be multiplication in the frequency domain. Performing two Fast Fourier Transforms (FFTs), multiplying the results, and then performing one Inverse FFT (IFFT) is computationally faster than performing one correlation between the two signals and provides the same result.

Let $x(t)$ denote the detector output. If no signal is present then $x(t)$ is just a realisation of noise $n(t)$, i.e. $x(t) = n(t)$, while in the presence of a deterministic signal $h(t)$ it takes the form,

$$x(t) = \mathrm{h}(\mathrm{t} - t_a) + n(t), \tag{1.13}$$

where $\mathrm{h}(\mathrm{t} - t_a)$ is a signal that simply shifts the signal relative to the origin of time. t_a is called time-of-arrival.

The correlation $\boldsymbol{c}$ of a template $q(t)$ with the detector output is defined as

$$c \equiv \int_{-\infty}^{\infty} x(t)q(t)dt. \tag{1.14}$$

The purpose of the above correlation integral is to improve the visibility of the signal. One can work out the ***optimal*** filter $q(t)$ that maximises the statistical average of the correlation $\boldsymbol{c}$ when a signal $h(t)$ is present in the detector output, very conveniently in the frequency domain. Write the correlation integral in the Fourier domain by substituting for $x(t)$ and $q(t)$, in the above integral, their Fourier transforms $\tilde{x}(f)$ and $\tilde{q}(f)$, i.e.,

$$x(t) \equiv \int_{-\infty}^{\infty} \tilde{x}(f)\exp(-2\pi ift)\,df, \tag{1.15a}$$

$$q(t) \equiv \int_{-\infty}^{\infty} \tilde{q}(f)\exp(-2\pi ift)\,df. \tag{1.15b}$$

After some routine algebra one obtains

$$c = \int_{-\infty}^{\infty} \tilde{x}(f)\tilde{q}^{*}(f)df, \tag{1.16}$$

where $\tilde{q}^{*}(f)$ denotes the complex conjugate of $\tilde{q}(f)$. In general, $\boldsymbol{c}$ consists of a sum of a two terms, a filtered signal $\boldsymbol{S}$ and filtered noise N:

$$c = S + N, \tag{1.17a}$$

$$\text{where, } S \equiv \int_{-\infty}^{\infty} \tilde{h}(f)q^{*}(f)e^{2\pi ift_a}df, \tag{1.17b}$$

$$\text{and, } N \equiv \int_{-\infty}^{\infty} \tilde{n}(f)q^{*}(f)df. \tag{1.17c}$$

If n is specified by a Gaussian random process with zero mean then $\boldsymbol{c}$ will also be described by a Gaussian distribution function, although its mean and variance will, in general, differ from those of n. The mean value of $\boldsymbol{c}$ is, clearly, $\boldsymbol{S}$ – the correlation of the template $\boldsymbol{q}$ with the signal h, since the mean value of n is zero:

$$\bar{c} = S = \int_{-\infty}^{\infty} \tilde{h}(f)\tilde{q}^{*}(f)e^{2\pi ift_a}df. \tag{1.18}$$

The variance of $\boldsymbol{c}$, that is $\overline{(c-\bar{c})^2}$, turns out to be,

$$\overline{(c-\bar{c})^2} = \overline{N^2} = \int_{0}^{\infty} S_h(f)\,|\tilde{q}(f)|^2\,df, \tag{1.19a}$$

$$\text{where, } \overline{\tilde{n}(f)\tilde{n}^{*}(f')} = S_h(f)\delta(f-f') \tag{1.19b}$$

$S_h(f)$ is the power noise spectral density of the detector. The power **SNR** is defined as

$$\rho^2 \equiv S^2/\overline{N^2}\,. \tag{1.20}$$

The amplitude **SNR** is ρ. The form of integrals in Eqs. *(1.18)* and (1.19a) motivates the definition of the scalar product of functions, which could either be templates or waveforms. Given two functions $a(t)$ and $b(t)$ we define their scalar product (a,b) to be

$$(a,b) \equiv 2\int_0^\infty \frac{df}{S_h(f)}\left[\tilde{a}(f)\tilde{b}^*(f) + \tilde{a}^*(f)\tilde{b}(f)\right]. \tag{1.21}$$

Recall that $S_h(f)$ is real and positive definite. Consequently, the above scalar product defines a positive definite norm: The norm of a, denoted $\|a\|$, is given by

$$\|a\| = 2\left[\int_0^\infty \frac{df}{S_h(f)}|\tilde{a}(f)|^2\right]^{1/2}. \tag{1.22}$$

The **SNR** in terms of the above scalar product is

$$\rho^2 = \frac{\left\langle he^{2\pi i f t_a}, S_h q\right\rangle^2}{\langle S_h q, S_h q\rangle}. \tag{1.23}$$

The scalar product of two functions (a,b) achieves its maximum value when $a = b$. Applying this, one finds that the template q that maximises p, called the ***optimal template,*** denoted $\tilde{q}_{\rm opt}(f)$, is simply

$$\tilde{q}_{\rm opt}(f) = \gamma\frac{\tilde{h}(f)e^{2\pi i f t_a}}{S_h(f)}, \tag{1.24}$$

where y is an arbitrary constant. The inverse Fourier transform of Eq.(1.24) gives the optimal template $q_{\rm opt}(t)$ in the time-domain.

$q_{\rm opt}(t)$ is the correlation of the ***time-translated*** signal $h(t)$ with the inverse Fourier transform of $1/S_h(f)$. To achieve the maximum SNR the optimal template has to not only match the shape of the signal but also its time-of-arrival t_a. The time-of-arrival of the signal will not be known before hand and one will have to construct the correlation of the detector output for several different relative lags of the template with respect to the detector output. In other words, one constructs the correlation function $c(t')$,

$$c(t') \equiv \qquad x(t)q(t-t')dt = \int_{-\infty}^{\infty}\tilde{x}(f)\tilde{q}^*(f)e^{-2\pi i f t'}df\,, \tag{1.25}$$

where t' is called the lag parameter.

The success of matched filtering requires an accurate model of signal. This is what

favours sources like ICB (NS-NS, BH-BH, NS-BH) over supernovae. In section 1.10 we provide a brief summary of gravitational wave phasing which forms the basis of GW data analysis for ICB's. In the following section we discuss elements of parametr estimation that we will require to investigate tests of GR using GW observations in the last two chapters.

1.9 Parameter estimation

The process of parameter estimation refers to the extraction of parameters which characterize the signal. Let the signal be $h(\theta^k)$, where θ^k for different values of k correspond to the different parameters. Hence one can view the signal to be a vector whose coordinates are θ^k. No estimation of parameters in a measurement process, howsoever accurate, yields the actual parameters of the signal. This is because at any finite SNR, the presence of noise alters the input signal. In the geometric language, the signal vector is being altered by the noise vector and the sum of them, which is what the detector output records, lies outside the signal manifold [35, 36].

Techniques such as matched filtering aim at computing the best projection of this altered vector onto the signal space. If p be the dimension of the signal space, the true parameters of the signal are expected to lie within an ellipsoid of p dimensions at a certain level of confidence – the volume of the ellipsoid increasing with the level of confidence. The axes of the ellipsoid are the 1–σ uncertainties in the estimation of parameters. The confidence level corresponding to a 1–σ uncertainty is 0.67^p, 2–σ uncertainty is 0.95^p, and so on [37].

This work begins with the assumption that gravitational waves from an inspiralling binary have been observed; i.e, that the appropriate detection criterion has been met by the detector output. We then discuss how to determine the parameters of an inspiralling binary system that best fit the measured signal. The set of all gravitational waveforms from two inspiralling bodies can be characterized by some number of parameters. For a given incident gravitational wave, different realizations of the noise will give rise to somewhat different best-fit parameters. However, for large SNR, the best-fit parameters will have a Gaussian distribution centered on the correct values. Specifically, let θ^i be the correct values of the parameters on which the waveforms depend, and let $\theta^i + \Delta\theta^i$ be the best fit parameters in the presence of some realization of the noise. Then for large SNR, the probability that the GW signal $s(t)$ is characterized by a given set of values of the source parameters θ^i is

$$p(\theta) = \mathcal{N} e^{-\frac{1}{2}\Gamma_{ij}\Delta\theta^i\Delta\theta^j}, \tag{1.26}$$

where Γ_{ij} is the so-called Fisher information matrix

$$\Gamma_{ij} = 2\int_0^\infty \left[\tilde{h}_i(f)\tilde{h}_j^*(f) + \tilde{h}_i^*(f)\tilde{h}_j(f)\right]\frac{df}{S_h(f)}\,, \tag{1.27}$$

where $\tilde{h}_i \equiv \frac{\partial\tilde{h}}{\partial\theta^i}$, with $\tilde{h}(f)$ being the Fourier transform of $h(t)$. The quantity $S_h(f)$ is the one-sided noise power spectral density (PSD) of the detector with units of Hz^{-1}; it is the only characteristic of the detector that enters the calculation of the errors in the estimation of parameters. $\mathrm{N} = \sqrt{\det(\Gamma/2\,\pi)}$ is the appropriate normalization factor. The variance-covariance matrix Σ^{ij} is given by

$$\Sigma^{ij} \equiv \langle\Delta\theta^i\Delta\theta^j\rangle = (\Gamma^{-1})^{ij}, \tag{1.28}$$

where $\langle\Delta\theta^i\Delta\theta^j\rangle$, the average over the probability distribution function, is given in Eq. (1.26). In terms of Σ^{ij}, the root-mean- square error in θ^i then is

$$\sqrt{\langle(\Delta\theta^i)^2\rangle} = \sqrt{\Sigma^{ii}}\,. \tag{1.29}$$

The correlation coefficient c^{ij} between parameters θ^i and θ^j is given by

$$c^{ij} = \frac{\Sigma^{ij}}{\sqrt{\Sigma^{ii}\Sigma^{jj}}}\,. \tag{1.30}$$

In the above equations, there is ***no*** summation over the repeated indices. By the definition of the correlation coefficient in Eq. (1.30), it is evident that it lies in the range $[-1, 1]$. A correlation coefficient value close to 1 (-1) would mean the parameters are completely correlated (anti-correlated). When the value is close to 0 then the two parameters are uncorrelated. Physically, if the correlation coefficient is close to ± 1, it means that one cannot produce two distinct signal shapes by varying both the parameters and varying one would be sufficient. Thus correlation coefficients are useful to see the extent to which the parameters are actually ***independent*** of each other.

1.10 Newtonian phasing - Adiabatic approximation

At the Lowest Quadrupolar or Newtonian order, the GW polarisations are given by

$$h_{+,\times} = \frac{2G\mu}{c^2R}\; x\; H^{(0)}_{+,\times} \tag{1.31a}$$

$$H^{(0)}_{+} = -(1 + c_i^2)\cos 2\phi, \tag{1.31b}$$

$$H^{(0)}_{\times} = -2c_i \sin 2\phi, \tag{1.31c}$$

in terms of the invariant Variable $x = \mathrm{v}^2$ where

$$x = \left(\frac{Gm\omega_{\rm orb}}{c^3}\right)^{2/3}$$

To study the evolution of the GWF under radiation-reaction, one must compute $x(t)$ and $\phi(t)$. Following [38] in the adiabatic approximation ($\frac{\omega}{\omega^2} << 1$) one begins from E, the CM energy at Newtonian order and $\mathcal{L}$, GW luminosity or energy flux

$$E = -\frac{1}{2}\mu c^2 x \tag{1.32a}$$

$$\mathcal{L} = \frac{32}{5}\frac{c^5}{G}\nu^2 x^5, \quad \frac{c^5}{G} \approx 3.63 \times 10^{52}\ \mathrm{W}, \tag{1.32b}$$

and the heuristic energy balance equation

$$\frac{dE}{dt} = -\mathcal{L}. \tag{1.33}$$

From them, one derives

$$x(t) = \frac{1}{4}\tau^{-1/4}, \tag{1.34a}$$

$$\tau = \frac{c^3\nu}{5Gm}(t_c - t), \tag{1.34b}$$

$$\phi = \int \omega dt = -\frac{5}{\nu}\int x^{2/3} d\tau, \tag{1.34c}$$

$$\phi_{\rm c} - \phi(t) = \frac{1}{\nu}\tau^{5/8}. \tag{1.34d}$$

From the above formula one can get an estimate of the PN order required to successfully match filter an ICB. For, the number of GW cycles N left until coalescence starting at some frequency ω is given by

$$\mathcal{N} = \frac{\phi_{\rm c} - \phi}{\pi} = \frac{1}{32\,\pi\,\nu}x^{-5/2} \tag{1.35}$$

$\propto (v/c)^{-5}$ (the inverse of $(v/c)^5$ the leading order at which radiation reaction begins). This yields $\sim$ 16000 cycles for NS-NS binaries. Matched filtering requires accuracy to about fraction of a cycle. Thus formally one needs to go to relative order 2.5PN or 3PN in $\mathcal{L}$ to achieve the required accuracy. Detailed work on GW data analysis confirms this [39, 34, 26, 40, 41, 42]. In the usual notation, nPN means corrections to lowest Newtonian result of order; $(v^2/c^2)^n = (v/c)^{2n}$. Currently all data analysis based on 2PN templates computed in Blanchet, Damour, BRI, Will and Wiseman [43]. To go beyond Post-Newtonian results one can use resummation methods based on Padé approximants [39]. To go beyond the adiabatic approximation one can use the effective-one-body approach (EOB) [24, 25, 44] or complete

approximants [45]. The extension to elliptical orbits upto 2PN is available in the works of Gopakumar and collaborators [46, 47]. The spinning case has been discussed in [48]. There is an extension of EOB to the spinning case by [49]

All the above works refer to the general binary case. In the test particle case more accurate results are available using perturbation methods in black hole spacetimes. In this case the exact (rather than a PN expanded) energy function is known. The energy flux is known to order 5.5PN analytically for circular orbits and up to 4PN for elliptical orbits. The exact energy flux is also known numerically for circular orbits in the adiabatic approximation. [50, 51].

1 . 1 GW from ICB - Three modules

From the discussions above it is clear that the computation of GWs in the adiabatic approximation involves three independent modules:

1. Motion: Given a binary system, iterate Einstein's field equations to discuss conservative motion of the system. Compute the conserved energy E.

2. Generation: Given the motion of the binary system on a fixed orbit, iterate the field equations to compute the multipoles of the gravitational field and hence the far-zone flux of energy and angular momentum carried by gravitational waves. Compute $\mathcal{L}$.

3. Radiation Reaction: Given the conserved energy and radiated flux of energy (and AM), assume the balance equations to compute the effect of radiation on the orbit. Compute $x(t)$ and $\phi(t)$.

GW phasing of a binary is similar to the EMW timing of pulsars. The heuristic assumption of energy balance circumvents the task of computing the EOM to very high PN order in the adiabatic approximation. In the above Newtonian phasing the EOM was required to ***only*** Newtonian accuracy. The use of the flux formula at 2.5PN leads to a correction to Newtonian acceleration of relative order 2.5PN. The complete treatment of the EOM to this order would require one to also control the 1PN and 2PN terms which is substantially more difficult as known from the binary pulsar analysis. An exact solution is impossible and one must resort to approximation methods.

1.12 Approximation methods

The most important approximation methods to compute GWs include:

1. Linear perturbations about non-flat background: μ-expansion
2. Post-Newtonian method or (non-linear): $\frac{1}{c}$ expansion (PNA)
3. Post-Minkowskian method or non-linear iteration: G-expansion (PMA)
4. Multipole decomposition in irreducible representation of the rotation group: (a-expansion in source radius)
5. Far zone expansion: $\frac{1}{R}$ expansion

Successful wave-generation formalisms employ a mix from the above options. A few comments regarding the various approximation is provided next.

The PN approximation is valid under assumption of weak gravitational field inside the source (weakly stressed) and slow internal motion. Its domain of validity is limited to the near zone of the source i.e. exterior region small w.r.t wavelength of the waves. ***A priori*** it is unable to incorporate the (no incoming) boundary conditions at infinity.
The PM approximation for weakly self gravitating sources is uniformly valid all over space-time. The PM approximation is a more general approximation relative to the PN approximation, multipole approximation and far-zone approximation. Each of the latter can be implemented at the second stage after the PM approximation is implemented as the first stage.

The multipole expansion is a very useful tool in physics. It is an expansion using spherical harmonics in the scalar case. Its use in GR is complicated due to two reasons. First, gravity is a tensorial (spin two) field requiring the use of tensor spherical harmonics. Tensor spherical harmonics are more complicated objects than the usual spherical harmonics. Symmetric trace fee (STF) tensors are equivalent to tensor spherical harmonics but more convenient to use and invariably employed. Second, GR is a non-linear theory. It requires additional tools and introduces new features like tails and other non-linear effects.

For stationary sources, multipole moments in the far field are given by convergent expansion of metric at spatial infinity [52, 53, 54, 55]. For non-stationary sources the first approach involves the expansion at future null infinity. The decomposition of the Bondi news function leads to the notion of the radiative moments [56, 57, 58]. The second approach involves combining multipole expansion with weak field or PM expansion [59, 60]. One views the multipole moments as source moments [54, 61, 62, 63]. Though the first Bondi-Sachs-Penrose approach is very powerful, it can address only part of the problem (the

field at infinity). It cannot be connected directly to features of the source. Hence we follow the second approach and adopt the multipole expansion within the complete non-linear theory following the Multipolar post Minkowskian formalism initiated by Blanchet and Damour [61, 62, 64, 63].

1.13 Model of the source and regularisation of the self-field

An accurate relativistic description of binary neutron stars or binary black holes requires a general method for dealing with the gravitational interaction of two (non-spinning) compact bodies; bodies whose radii are of the same order as their gravitational radii. During his careful analysis of the binary pulsar 1913+16 Damour [65] introduced a matching approach which combined two different approximation methods: (i) "external perturbation scheme": an iterative, weak-field (post-Minkowskian) approximation scheme valid in a domain outside two world-tubes containing the two bodies. (ii) "internal perturbation scheme": a scheme describing the small perturbations of each body by the far-field of its companion. He showed that to a very high approximation, the internal structures of the compact bodies are *effaced* when seen in the external scheme. The internal structure effects the EOM only starting at 5PN level ($1/c^{10}$). (Physically, it is due to the influence on the orbital motion of Newtonian quadrupole moments induced by tidal interaction between the two compact objects.) The effacement result is the rationale for describing, up to 5PN order, two (non spinning) compact bodies in terms of two point masses. Mathematically we represent the compact bodies by a "skeleton" made of two massive world-lines described by a point-particle action

$$S_{\rm pp} = -\sum_a m_a c \int \sqrt{-g_{\mu\nu}(y_a^\lambda)\, dy_a^\mu\, dy_a^\nu}\,. \tag{1.36}$$

Thus, non-spinning compact objects can be well modeled as point particles described by 6-functions governed by gravitation, described by GR. This allows a systematic analytical approximation scheme for the calculation of associated waveforms to the order required or resources permit. However, there is a technical problem to be overcome: How to handle delta functions in a non-linear theory? This requires the use of a regularization scheme for the self field.

1.14 Post-Newtonian wave generation

The generation of problem in gravitational radiation theory refers to the problem of relating the outgoing gravitational wave field to the structure and motion of the material source. The gravitational wave generation problem is important to decode source characteristics from the signals that gravitational wave detectors are likely to receive. The main complication is due to non-linear effects of gravitation.

The standard quadrupole equation was first derived by Einstein [66] within the linearized approximation to general relativity and is applicable only to slowly moving sources with negligible self gravity. Consequently, it does not apply to any realistic astrophysical system since e.g., it cannot be applied to a binary system of two ordinary stars whose motion is governed by gravitational forces. Hence these equations need to be generalized to at least weakly self-gravitating systems. This was achieved along two very different lines by Landau-Lifshitz [67, 68] and Fock [69] respectively. Epstein and Wagoner [70] studied post-Newtonian corrections. The Landau-Lifshitz approach has been followed up by Thorne [71, 54], Anderson [72] and Walker and Will [73]. In particular Thorne [71, 54] has developed a formalism for calculating gravitational radiation from slow motion sources (not necessarily weakly self-gravitating) by a systematic use of multipole decomposition and formal inclusion of higher order multipoles. However, all this work was unsatisfactory as it involved both at the intermediate steps and in the final results undefined divergent integrals. This is because all this work makes essential use of the Landau-Lifshitz effective stress tensor of the gravitational field which is not confined to the compact support of the source but extends with a slow falloff to infinity [74].

Fock's approach is conceptually different and lends itself to useful generalizations. The main idea is to solve the problem in two parts. First, compute the gravitational field in the near zone of the source where retardation is small compared to the characteristic period. Next, obtain the structure of the general radiative gravitational field in the wave zone. Finally, match the results of the two steps via an intermediate expression for the gravitational field that bridges the gap between the two zones. The Multipolar post Minkowskian formalism due to Blanchet, Damour and collaborators [61, 62, 63, 75, 76, 77] based on the Fock approach is the most refined and successful formalism at present. Currently it is the only appproach complete up to 3PN both in the EOM and radiation problems. It builds on the earlier work of Bonnor and collaborators [78, 59, 60] and Thorne [54].

Using the ***Direct Integration of Relaxed Einstein Equations (DIRE)*** Will and Wiseman [79] set up an improved Epstein-Wagoner-Thorne formalism which dealt with the problem of divergences differently from the MPM formalism. It is equivalent to the MPM formalism [7] but an algebraically different implementation, thus providing an useful check on the final

formulas. However, currently DIRE is complete only up to 2PN in EOM and generation. The Landau-Lifshitz approach was improved by Futamase and Schutz [80] while Futamase [81] extended it to sources with strong self-gravity but weak mutual self-gravitation. Though this approach has derived the 3PN EOM [82] for generation it has been investigated only at the leading Newtonian order.

The generation problem beyond the lowest linearised gravity involves two independent aspects addressing two independent problems. First, the setting up of a general method applicable to extended or fluid sources with compact support based on the mixed post-Minkowskian approximation and multipole expansion (MPM) and matching to some post-Newtonian source. Second, the application to point particle binaries modelling **ICB's**, using a choice of a regularization scheme for the self-field. The various schemes used in the literature include: Pure Hadamard Schwarz regularization, Riesz regularization, Extended Hadamard regularization and more recently Dimensional regularization.

The 2.5PN point-particle description was dealt by using Riesz analytical continuation method to (uniquely) regularize the divergent integrals linked to the use of point particles in non-linear general relativity [83, 84]. Equivalent results could be obtained by using an analytic continuation of the space-time dimension D, instead of a Riesz-type analytic continuation. Surprisingly, the 3PN order turned out to be technically complicated and it was almost ten years before the situation has become conceptually satisfactory. Using Hadamard-type regularizations most of the complicated non-linear integrals appearing at 3PN order could be unambiguously dealt with. However, a few of them turned out to be ambiguous because of the appearance of logarithmic divergences at the 3PN order These led to 4 undetermined coefficients at 3PN:

One in the 3PN acceleration [85, 86, 87, 88, 44, 89, 90, 91, 92, 93, 94, 95], ω_s or $\lambda = -\frac{3}{11}\omega_s - \frac{1987}{3080}$

$$\vec{a}_1 = -\frac{Gm_2\vec{n}_{12}}{r_{12}^3} + \frac{\cdots}{c^2} + \frac{\cdots}{c^4} + \frac{\cdots}{c^5} \tag{1.37}$$

$$+\frac{1}{c^6}\left[\ldots + (\text{gauge dependent})\ln r_{12} - \frac{44}{3}\lambda\frac{G^4(m_1+m_2)m_1m_2^2}{r_{12}^5}\vec{n}_{12}\right] \tag{1.38}$$

and three in the 3PN mass quadrupole moment [95, 96], ξ, ζ and κ,

$$I_{ij} = \ldots + \frac{44}{3}\frac{G^2m_1^3}{c^6}\left[\left(\xi + \kappa\frac{m_1+m_2}{m_1}\right)a_1^{(i}y_1^{j)} + \zeta v_1^{(i}v_1^{j)}\right] + 1 \leftrightarrow 2$$

1.15 Multipolar post Minkowskian method

The Multipolar post Minkowskian formalism due to Blanchet and Damour [61, 62, 64, 63] proceeds as follows:

- First: Desdribe the gravitational field in the region exterior to a general isolated system by a Multipolar Post Minkowskian metric. Assume the metric is stationary in the neighbourhood of past timelike infinity and asymptotically Minkowskian in the past. The general method for the external field is not limited a priori to slowly moving PN sources. In the construction of the external field the divergence at the origin arising from the use of the (external) multipolar expansion must be carefully controlled. In the MPM approach this is implemented using an analytic continuation finite part operation. This plays a crucial role in the construction of the PM iteration to any order.

- Second: Relate the multipole moments to the material content of source. In Linearized gravity the above relation is independent of source velocity. However, it is not so in the non-linear theory. Hence one must supplement MPM by an assumption of the metric inside the isolated system. One assumes the metric is regular and smooth and admits inside a post-Newtonian expansion that matches to the vacuum MPM metric in the exterior (in the sense of asymptotic expansions). In other words, there should exist a 'matching' or 'overlapping' region where both the MPM and PN expansions are valid. For slowly moving and weakly stressed i.e. PN sources this region always exists and is the exterior ($r > a$) near ($r \ll A$) zone. ($a < r \ll A$). Hence, closed form expressions for source multipole moments can only be obtained for PN sources with the typical internal velocity as the small PN parameter.

- Third: In a non-linear theory the source multipole moments mix with each other causing non-linear effects in the radiation field. One must then relate the source moments to the radiative moments

- General structure of the PN expansion ($c \to +\infty$) is necessarily of the type

$$h_n(c) \simeq \sum_{p,q\in\mathbb{N}} \frac{(\ln c)^p}{c^q}, \tag{1.39}$$

  where $p \leq n-1$ (and $q \geq 2$). PN expansion involves not only with the normal powers of $1/c$ but also powers of the logarithm of c

1.16 General source moments, canonical source moments and radiative moments

The end result of the implementation of the above computations are the expression for the six general source moments [97, 98]. The most important 'mass' and 'current' moments are given by:

$$I_L(t) = \underset{B=0}{\mathrm{FP}} \int d^3\mathbf{x}\, |\tilde{\mathbf{x}}|^B \int_{-1}^{1} dz \left\{ \delta_l(z)\hat{x}_L \Sigma - \frac{4(2l+1)}{c^2(l+1)(2l+3)} \delta_{l+1}(z)\hat{x}_{iL}\dot{\Sigma}_i + \frac{2(2l+1)}{c^4(l+1)(l+2)(2l+5)} \delta_{l+2}(z)\hat{x}_{ijL}\ddot{\Sigma}_{ij} \right\} (\mathbf{x}, t + z|\mathbf{x}|/c) , \quad (1.40)$$

$$J_L(t) = \underset{B=0}{\mathrm{FP}}\, \varepsilon_{ab<i_l} \int d^3\mathbf{x}\, |\tilde{\mathbf{x}}|^B \int_{-1}^{1} dz \left\{ \delta_l(z)\hat{x}_{L-1>a}\Sigma_b - \frac{2l+1}{c^2(l+2)(2l+3)} \delta_{l+1}(z)\hat{x}_{L-1>ac}\dot{\Sigma}_{bc} \right\} (\mathbf{x}, t + z|\mathbf{x}|/c) . \quad (1.41)$$

In the above,

$$\tau^{\alpha\beta} = \underbrace{|g|T^{\alpha\beta}}_{\text{matter term}} + \underbrace{\frac{\mathbf{c}^4}{16\pi G}\Lambda^{\alpha\beta}}_{\text{grav. source term}}, \quad (1.42a)$$

(1.42b)

$$\begin{aligned} \Lambda^{\alpha\beta} = {} & -h^{\mu\nu}\partial^2_{\mu\nu}h^{\alpha\beta} + \partial_\mu h^{\alpha\nu}\partial_\nu h^{\beta\mu} + \frac{1}{2}g^{\alpha\beta}g_{\mu\nu}\partial_\lambda h^{\mu\tau}\partial_\tau h^{\nu\lambda} \\ & - g^{\alpha\mu}g_{\nu\tau}\partial_\lambda h^{\beta\tau}\partial_\mu h^{\nu\lambda} - g^{\beta\mu}g_{\nu\tau}\partial_\lambda h^{\alpha\tau}\partial_\mu h^{\nu\lambda} + g_{\mu\nu}g^{\lambda\tau}\partial_\lambda h^{\alpha\mu}\partial_\tau h^{\beta\nu} \\ & + \frac{1}{8}(2g^{\alpha\mu}g^{\beta\nu} - g^{\alpha\beta}g^{\mu\nu})(2g_{\lambda\tau}g_{\epsilon\pi} - g_{\tau\epsilon}g_{\lambda\pi})\partial_\mu h^{\lambda\pi}\partial_\nu h^{\tau\epsilon}, \end{aligned} \quad (1.42c)$$

$$\overline{\tau}^{\mu\nu} = \mathrm{PN}(\tau^{\mu\nu}), \quad (1.42d)$$

$$\Sigma = \frac{\overline{\tau}^{00} + \overline{\tau}^{ii}}{c^2} ; \quad \Sigma_i = \frac{\overline{\tau}^{0i}}{c} ; \quad \Sigma_{ij} = \overline{\tau}^{ij}, \quad (1.42e)$$

$$\delta_l(z) = \frac{(2l+1)!!}{2^{l+1}l!}(1-z^2)^l ; \quad \int_{-1}^{1} dz\delta_l(z) = 1 . \quad (1.42f)$$

To compute the multipole moments to a given PN order one performs a retardation expansion of the above equations using:

$$\int_{-1}^{1} dz\delta_l(z)S(\mathbf{x},t+z|\mathbf{x}|/c) = \sum_{j=0}^{\infty} \frac{(2l+1)!!}{2^j j!(2l+2j+1)!!}|\mathbf{x}|^{2j}\left(\frac{\partial}{c\partial t}\right)^{2j} S(\mathbf{x},t). \quad (1.43)$$

In the linearised gravity case the above results reduce to the results in Damour and Iyer [99, 100] as required.

The explicit computation of the moments can be schematically summarised thus. The source moments I_L J_L are functions of $\bar{}\Sigma$, Σ^i, Σ^{ij}, which in turn are functions of the total stress-energy tensor $\bar{}\tau$ which can be expressed in terms of the metric perturbations $\bar{}$ h. To proceed, one must express h in terms of retarded potentials [96] or further in terms of Poisson like potentials [95]. By an integration by parts one can simplify some terms to simpler surface terms, using Leibniz rule (valid for smooth sources). The computation of the multipole moments to 3PN is very long and involves tens of thousands of terms.

Starting from the complete six STF Source Moments I_L, J_L, W_L, X_L, Y_L, Z_L, for which general expressions can be given valid to any PN order, one can define a set of Two Canonical source moments M_L and S_L such that the two sets of moments are physically equivalent i.e metrics constructed from them differ by a coordinate transformation. Thus, by a gauge transformation one can go from

$$(I_L, J_L, \ldots, Z_L) \rightarrow (M_L, S_L, 0 \ldots 0)$$

$$\text{s.t. } h^{\alpha\beta}\ [I_L, \ldots, Z_L] \text{ is isometric to } k^{\alpha\beta}[M_L, S_L]$$

The six general source moments are closely rooted to the source; we know them as integrals over $\tau^{\mu\nu}$. However, the canonical moments are necessary since they simplify the calculations of the external non-linearities. Their existence shows that any radiating isolated source characterised by *two* and only *two* sets of time-varying multipole moments. We need,

$$M_{ij} = I_{ij} - \frac{4G}{c^5}\left[W^{(2)}I_{ij} - W^{(1)}I^{(1)}_{ij}\right] + O(7), \quad (1.44)$$

$$W = \frac{1}{3}\int d^3\mathbf{x}\, x_i\sigma_i = \frac{1}{3}m_1(y_1v_1) + O(2) + 1 \leftrightarrow 2. \quad (1.45)$$

The MPM formalism is valid all over the weak field region outside the source including wave-zone (upto future null infinity) in harmonic coordinates. The far zone expansion at Minkowskian future null infinity has the structure

$$\sum \frac{\hat{n}_L(\ln r)^p}{r^k} G_{L,k,p,n}(u).$$

One can define step by step in **PM** expansion, ***Radiative coordinates*** by gauge transformation to eliminate these Log terms. One recovers Bondi-type radiative metric [64]. One can then extract ***Radiative Moments*** U_L and V_L in the standard way:

$$H_{ij}^{\rm TT}(U,\mathbf{N}) = \frac{4G}{c^2R}\mathcal{P}_{ijab}(\mathbf{N})\sum_{l=2}^{+\infty}\frac{1}{c^l l!}\Big\{N_{L-2}\,U_{abL-2}(U) - \frac{2l}{c(l+1)}N_{cL-2}\varepsilon_{cd(a}\,V_{b)dL-2}(U)\Big\} + O\left(\frac{1}{R^2}\right).$$

The two ***radiative*** multipole moments U_L and V_L can be obtained as some non-linear functional of the two ***canonical*** moments M_L and S_L and thus of the six general ***source*** moments I_L, J_L, W_L, X_L, Y_L, Z_L. The non-linearities in the external field are computed by the **PM** algorithm. The relation between the radiative and source moments include many non-linear multipole interactions as the source moments mix with each other as the wave propagates from source to detector.

$$U_L(U) = M_L^{(l)}(U) + \frac{2GM}{c^3}\int_0^{+\infty}d\tau\; M_L^{(l+2)}(U-\tau)\left[\ln\left(\frac{c\tau}{2r_0}\right)+\kappa_l\right] + O\left(\frac{1}{c^5}\right), \tag{1.46}$$

$$V_L(U) = S_L^{(l)}(U) + \frac{2GM}{c^3}\int_0^{+\infty}d\tau\; S_L^{(l+2)}(U-\tau)\left[\ln\left(\frac{c\tau}{2r_0}\right)+\pi_l\right] + O\left(\frac{1}{c^5}\right), \tag{1.47}$$

In the above κ_l and π_l are constants that are given by general formulas in [97].

$$\begin{aligned} U_{ij}(T_R) = {} & \left[M_{ij}^{(2)}(T_R) + \frac{G}{c^5}\left\{\frac{1}{7}M_{a<i}^{(5)}M_{j>a} - \frac{5}{7}M_{a<i}^{(4)}M_{j>a}^{(1)} - \frac{2}{7}M_{a<i}^{(3)}M_{j>a}^{(2)} + \frac{1}{3}\varepsilon_{ab<i}M_{j>a}^{(4)}S_b\right\}\right] \\ & + \left[\frac{2Gm}{c^3}\left\{\int_{-\infty}^{T_R}dV\left[\ln\left(\frac{T_R-V}{2b}\right)+\frac{11}{2}\right]M_{ij}^{(4)}(V)\right\} + \frac{G}{c^5}\left\{-\frac{2}{7}\int_{-\infty}^{T_R}dV M_{a<i}^{(3)}(V)M_{j>a}^{(3)}(V)\right\}\right] + \\ & + \frac{2G^2m^2}{c^6}\int_0^{+\infty}d\tau M_{ij}^{(5)}(t-\tau)\left[\ln^2\left(\frac{c\tau}{2r_0}\right)+\frac{57}{70}\ln\left(\frac{c\tau}{2r_0}\right)+\frac{124627}{44100}\right] + O(7). \end{aligned} \tag{1.48}$$

The radiative mass-type quadrupole moment U_{ij} includes a quadratic tail at the relative

1.5PN order (or $1/c^3$). It represents the interaction of the mass M of the source and its quadrupole moment I_{ij}. Physically, it represents the back-scattering of quadrupolar waves off the Schwarzschild curvature generated by M. It gives the dominant non-linear effect of tails and will appear at 4PN order in the EOM beyond Newtonian acceleration. U_{ij} also includes the non-linear memory integral at the 2.5PN order. It represents quadrupolar radiation of the stress-energy distribution of linear quadrupole waves themselves, the multipole interactions $I_{ij} \times I_{kl}$. Cubic tail, or "tail of tail", arising at the 3PN order, corresponds to the multipole interaction $M^2 \times I_{ij}$. The computation of tail integrals require a model for the orbit since it depends on the behaviour of the field at all instants in the past. One can use a non-decaying circular orbit in those cases where the remote past contribution to tail integrals can be shown to be negligible.

1.17 Application to compact binary systems

In the application of the above results to compact binary systems, the second aspect of our approach comes into play. NS or BH are modelled as point particles represented as Dirac δ-functions bringing along the technical problem of how to handle δ– fns in a non-linear theory. The general formalism set up for continuous smooth matter distribution with continuous $T^{\mu\nu}$ cannot be directly applied to point particles since they lead to ***divergent*** integrals at location of particles when $T^{\mu\nu}_{\text{point-particle}}$ is substituted in the source moments I_L, J_L, W_L, X_L, Y_L, Z_L. The formulas need to be supplemented by a prescription for removing the ***infinite self field*** of point particles. This is our ***ansatz*** for applying a well-defined general 'fluid' formalism to an ill-defined point-particle source. It is implemented by the use of one of the following regularisation schemes: Pure Hadamard regularisation (HR) based on Hadamard's partie finie, Riesz regularisation, Extended Hadamard regularisation or Dimensional regularisation (DR)

In both the Amowitt-Deser- Misner (ADM) and harmonic approaches to 3PN dynamics and MPM approach to radiation, the use of Dirac-delta-function sources to model the two-body system causes the appearance of both badly divergent integrals and badly defined "contact terms" which cannot be unambiguously regularized by Hadamard regularisation or Riesz regularisation. The incompleteness of Hadamard Regularisation at 3PN leads to appearance of ***Ambiguity*** parameters (arbitrary dimensionless coefficient whose value cannot be fixed within Hadamard Regularisation). Hadamard regularization of the self-field of point particles violates the gauge symmetry of perturbative general relativity (diffeomorphism invariance) and thereby breaks the crucial link between Bianchi identities and EOM. This is probably why the Hadamard based works are unable to fix the parameter ω_s, λ, ξ, κ, ζ

Dimensional regularisation was introduced by 't Hooft & Veltrnan [101] to respect gauge

symmetry of perturbative quantum gauge theories. Here we use it to respect gauge symmetry associated with diffeomorphism or general coordinate invariance of classical general relativistic description of interacting point masses Work in d + 1 spacetime dimensions, where d considered as a continuous complex number. If d = (3 – A) this regularisation is equivalent to the successful Riesz regularisation upto 2.5PN. Dimensional Regularization respects the gauge symmetry of perturbative GR. In this sense, it is a better regularization scheme.

One has to redo all calculations from the beginning in d + 1 dimensions with all the d-dependent coefficients. One then computes the Difference between the $d-$ dimensional Dimensional Regularisation result and 3 dimensional one corresponding to Hadamard regularisation (pure Hadamard-Schwartz). The difference is computed in the form of a Laurent expansion in ε = d – 3. The ε expansion of the difference depends only on the singular behaviour of metric coefficients in the vicinity of point particles. Hence functions involved in the delicate divergent integrals can be computed in $d-$ dimensions as local expansions in the 'sizes' r_1 or r_2. Ambiguities arise solely from terms in the integration region near the particles $r_1 \to 0$ or $r_2 \to 0$ that give rise to poles $\propto 1/\varepsilon$ where $\varepsilon \equiv$ d – 3 corresponding in 3 dimensions to logarithmic ultraviolet divergences. The difference $\mathcal{D}I$ between the DR evaluation of the d-dimensional local integral and its corresponding three-dimensional (pure) HS one is expressible in terms of the ε- expansion coefficients. Imposing the physical equivalence between the DR result and HR one determines all the ambiguity parameters. There are no undetermined parameters any more and the 3PN EOM and radiation are complete and available for use in GW data analysis.

1.18 Current status

What is the current status of the computations of the equation of motion (EOM) and energy flux (luminosity) in the general binary case for ICB binaries? The energy E or equivalently EOM is known to 3PN accuracy for general orbits. It has been computed by three independent methods. The first two are ADM Hamiltonian method using Hadamard regularisation (HR) by Damour, Jaranowski, Schafer [87, 88, 44, 89] and EOM in harmonic coordinates using HR by Blanchet and Faye [85]. The results were equivalent but included one ambiguity parameter λ or ω_s arising from the incompleteness of the Hadamard regularisation. By using dimensional regularisation both the groups independently determined the ambiguity parameter and checked their agreement. [87, 88, 44, 89, 102]. The third computation was the surface integral approach by Itoh and Futamase [82] for two spherical compact stars in harmonic gauge without introducing singular sources. The surface integral approach leads to EOM independent of internal structure. The 3.5PN terms in the EOM has also been computed by three independent groups [90, 91, 92, 93, 103, 104, 105, 106, 107]. In the case

of luminosity $\mathcal{L}$ or the energy flux, the results are known in the circular orbit case to 3.5PN accuracy relative to the to quadrupolar (Newtonian) order. It was computed using HR by Blanchet, Iyer and Joguet [95] and included three more undetermined ambiguity parameters arising due to the incompleteness of the Hadamard regularisation. The associated 3.5PN GW phasing was provided by Blanchet, Faye, Iyer and Joguet [108]. By using DR, Blanchet, Damour, Esposito-Farése and Iyer determined the three ambiguity parameters completing the 3PN generation [109]. Based on the above inputs the restricted GW templates can be computed to 3.5PN accuracy in the phase [108, 109]. This effectively deal with terms in the acceleration of orders $\sim$ 5.5PN /6PN term relative to the Newtonian accn. The complete GW templates including all the amplitude corrections is known to order 2.5PN beyond the lowest order Newtonian waveform has been computed by Arun, Blanchet, Iyer and Qusailah [110]. These final polarisations at 2.5PN can be schematically written as:

$$\begin{aligned} h_{+,\times} &= \frac{2Gm\nu x}{c^2 R}\Big\{H^{(0)}_{+,\times} + x^{1/2} H^{(1/2)}_{+,\times} + x H^{(1)}_{+,\times} + x^{3/2} H^{(3/2)}_{+,\times} \\ &\quad + x^2 H^{(2)}_{+,\times} + x^{5/2} H^{(5/2)}_{+,\times}\Big\} . \end{aligned} \tag{1.49}$$

Together with the 3.5PN phasing results quoted below these provide the best templates available today.

$$\begin{aligned} x(\tau) &= \frac{1}{4}\tau^{-1/4}\Big\{1 + \left(\frac{743}{4032} + \frac{11}{48}\nu\right)\tau^{-1/4} - \frac{1}{5}\,\pi\,\tau^{-3/8} \\ &+ \left(\frac{19583}{254016} + \frac{24401}{193536}\nu + \frac{31}{288}\nu^2\right)\tau^{-1/2} + \left(-\frac{11891}{53760} + \frac{109}{1920}\nu\right)\pi\,\tau^{-5/8} \\ &+ \left(-\frac{10052469856691}{6008596070400} + \frac{1}{6}\,\pi^2 + \frac{107}{420}\,C - \frac{107}{3360}\ln\left(\frac{\tau}{256}\right)\right. \\ &+ \left.\left[\frac{3147553127}{780337152} - \frac{451}{3072}\,\pi^2\right]\nu - \frac{15211}{442368}\nu^2 + \frac{25565}{331776}\nu^3\right)\tau^{-3/4} \\ &+ \left(-\frac{113868647}{433520640} - \frac{31821}{143360}\nu + \frac{294941}{3870720}\nu^2\right)\pi\,\tau^{-7/8}\Big\} . \end{aligned} \tag{1.50}$$

and

$$\begin{aligned} \phi(\tau) &= -\frac{1}{\nu}\Big\{\tau^{5/8} + \left(\frac{3715}{8064} + \frac{55}{96}\nu\right)\tau^{3/8} - \frac{3}{4}\,\pi\,\tau^{1/4} \\ &+ \left(\frac{9275495}{14450688} + \frac{284875}{258048}\nu + \frac{1855}{2048}\nu^2\right)\tau^{1/8} + \left(-\frac{38645}{172032} + \frac{65}{2048}\nu\right)\pi\,\ln\left(\frac{\tau}{\tau_0}\right) \\ &+ \left(\frac{831032450749357}{57682522275840} - \frac{53}{40}\,\pi^2 - \frac{107}{56}\,C + \frac{107}{448}\ln\left(\frac{\tau}{256}\right)\right. \\ &+ \left.\left[-\frac{126510089885}{4161798144} + \frac{2255}{2048}\,\pi^2\right]\nu + \frac{154565}{1835008}\nu^2 - \frac{1179625}{1769472}\nu^3\right)\tau^{-1/8} \end{aligned}$$

$$+ \left(\frac{188516689}{173408256} + \frac{488825}{516096}\nu - \frac{141769}{516096}\nu^2\right)\pi\,\tau^{-1/4}\Big\}\,, \tag{1.51}$$

where C = 0.577216 the Euler constant. The constant τ_0 is related to a constant phase that is simply fixed by the initial conditions when the frequency of the wave enters the detector's bandwidth.

$$\tau = \frac{\nu c^3}{5Gm}(t_c - t)\,, \tag{1.52}$$

where t_c denotes the instant of coalescence, at which the frequency tends formally to infinity (evidently, the approximation breaks down well before this point).

Table 1.1: The contributions to the accumulated number $\mathrm{N} = \frac{1}{\pi}(\phi_{\mathrm{ISCO}} - \phi_{\mathrm{seismic}})$ of gravitational-wave cycles [108, 109] at different PN orders for three prototypical systems. The frequency entering the bandwidth is $f_{\mathrm{seismic}} = 10$ Hz; terminal frequency is assumed to be at the Schwarzschild innermost stable circular orbit $f_{\mathrm{ISCO}} = \frac{c^3}{6^{3/2}\pi Gm}$.

	$2\times 1.4M_\odot$	$10M_\odot + 1.4M_\odot$	$2\times 10M_\odot$
Newtonian	16031	3576	602
1PN	441	213	59
1.5PN	−211	−181	−51
2PN	9.9	9.8	4.1
2.5PN	−12.2	−20.4	−7.5
3PN	2.6	2.3	2.2
3.5PN	−1.0	−1.9	−0.9

We conclude with a table 1.1 that gives the contributions to the accumulated number $\mathcal{N} = \frac{1}{\pi}(\phi_{\mathrm{ISCO}} - \phi_{\mathrm{seismic}})$ of gravitational-wave cycles [108, 109]. The frequency entering the bandwidth is $f_{\mathrm{seismic}} = 10$ Hz; terminal frequency is assumed to be at the Schwarzschild innermost stable circular orbit $f_{\mathrm{ISCO}} = \frac{c^3}{6^{3/2}\pi Gm}$.

From the table it is clear that we have the phasing accuracy we desire to deal with ICB in laser interferometric GW detectors.

1.19 Eccentric binaries

Inspiralling compact binaries are usually modeled as point particles in ***quasi-circular*** orbits. For long lived compact binaries, the quasi-circular approximation is quite appropriate, as the radiation reaction decreases the orbital eccentricity to negligible values by the epoch the emitted gravitational radiation enters the sensitive bandwidth of the interferometers. It is by now well-known that the gravitational waveform of an eccentric binary could be significantly different from that of a circular one and different detection strategies are required for optimal detections (e.g., [111, 112, 113, 114, 115, 116, 117].

Though the strongest and first sought binary sources of GW are those moving in quasi-circular orbits, there is a also interest in inspiralling binaries moving in ***quasi-eccentric*** orbits. Astrophysical situations currently do exist which lead to binaries with nonzero eccentricity in the gravitational wave detector bandwidth, both ground-based and space-based. Prominently, inner binaries of hierarchical triplets undergoing Kozai oscillations [118] may not only merge due to gravitational radiation reaction [119] but a good fraction (– 30%) of them will have eccentricity greater than about 0.1 as they enter the sensitivity band of advanced ground based interferometers. [120]. The majority of the above systems possess eccentricities well below 0.2 at 40 Hz and below 0.02 at 200 Hz. The population of stellar mass binaries in globular clusters is expected to have a thermal distribution of eccentricities [121]. As another example, in the study on the growth of intermediate BHs [122] in globular clusters it was found that the binaries have eccentricities between 0.1 and 0.2 in the LISA bandwidth.

Finally, if a Kozai mechanism is at work, supermassive black hole binaries could be in highly eccentric orbits and merge within the Hubble time [123]. Since supermassive black hole binaries are powerful GW sources for LISA, the effects of eccentricity would need to be carefully addressed. Sources of the kind discussed above provide the prime motivation to investigate higher post-Newtonian order modelling for quasi-eccentric binaries. In this thesis we compute the total energy flux or GW luminosity from inspiralling compact binaries moving in general orbits at the third post-Newtonian order. In addition to the instantaneous terms, the more involved hereditary terms depending on the past history of the binary also contribute and must be evaluated.

1.20 Gravitational wave recoil

1.20.1 What is gravitational wave recoil

Gravitational waves (GWs) carry energy and angular momentum from a binary system, causing decay of the binary's orbit and eventually driving the system to merge into a single object. GWs also carry ***linear*** momentum from the system as well (e.g., [124]). As a consequence, the center of mass in this case must recoil in order to satisfy global conservation of momentum. If the recoil velocity is comparable to or greater than the escape velocity of the binary's host structure, there could be important dynarnical consequences, such as ejection of the merged black hole remnant.

The recoil arises because the radiation field generated by a binary is typically asymmetric. Consider the following argument due to Alan Wiseman. In an unequal mass binary (Fig. 1.4), the smaller member, m_1, moves with a higher speed than the larger member, m_2. It

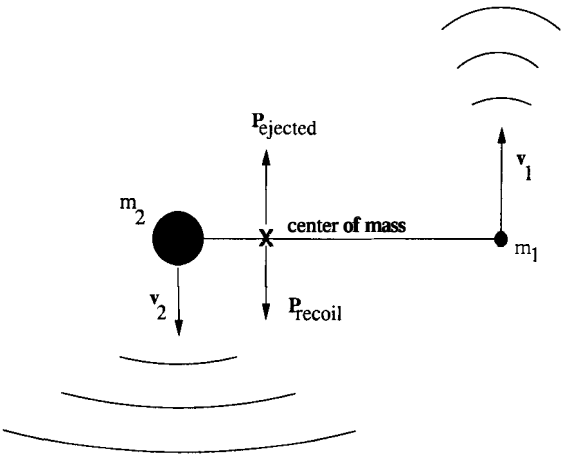

Figure 1.4: GW emission from an unequal mass binary. Momentum is ejected parallel to the smaller body's velocity ($\vec{v}_1$). Conservation of momentum requires that the system recoil in the opposite direction [8].

is thus more effective at "forward beaming" its wave pattern. This means that there is an instantaneous net flux of momentum ejected from the system parallel to the velocity of the smaller body, and a concomitant recoil opposing this [8].

Over an orbit, the recoil direction continually changes. If the orbit were perfectly circular, this means that there would be no net interesting effect — the binary's center of mass would run around in a circle, and the *net* recoil would sum to zero. However, when GW emission is strong, the orbit is *not* perfectly circular: Because of the secular, dissipative evolution of the binary's energy and angular momentum, the black holes slowly spiral towards one another. Since the orbit does not close, the recoil does not sum to zero. The recoil accumulates until the holes merge and settle down to a quiescent state, shutting off the momentum flux and yielding a net, non-zero kick.

This recoil is not a property unique to GWs — it holds for *any* form of radiation[3]. This can be simply seen by considering a multipolar decomposition. Consider a distribution of charges with non-zero electric dipole and quadrupole moments, as in Fig. 1.5. Spin this arrangement about its center point, causing the system to radiate electromagnetic waves. What does this radiation distribution look like from far away?

The radiation's *amplitude* has two pieces, dipole and quadrupole:

$$\vec{E} = \vec{E}^{\rm dip} + \vec{E}^{\rm quad}, \qquad \text{where} \tag{1.53}$$

$$\vec{E}^{\rm dip} \propto e^{i(\phi-\omega t)}, \qquad \vec{E}^{\rm quad} \propto e^{2i(\phi-\omega t)} \tag{1.54}$$

[3] Indeed, electromagnetic or neutrino recoil may impact neutron star kicks [125, 126].

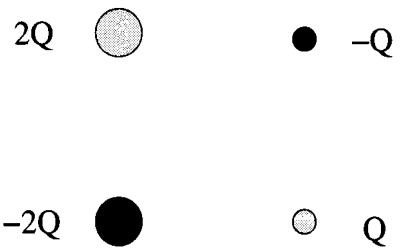

Figure 1.5: Charge distribution with non-zero dipole and quadrupole moment. Spinning this distribution about its center point produces radiation carrying non-zero linear momentum due to beating between the dipolar and quadrupolar radiation fields [8].

Since the intensity $\mathbf{I} \propto |\vec{E}|^2$, it will contain three pieces:

$$I = I^{\rm dip} + I^{\rm quad} + I^{\rm dip-quad} \,, \tag{1.55}$$

where

$$I^{\rm dip} \propto |\vec{E}^{\rm dip}|^2 \propto \text{constant} \,; \qquad I^{\rm quad} \propto |\vec{E}^{\rm quad}|^2 \propto \text{constant} \tag{1.56}$$

$$I^{\rm dip-quad} \propto \mathrm{Re}\left[\vec{E}^{\rm dip}\bar{\vec{E}}^{\rm quad}\right] \propto \cos(\phi - \omega t) \,. \tag{1.57}$$

The intensity has a preferred direction, which rotates as the charge distribution rotates. The energy from the system is instantaneously beamed in a preferred direction, and so there is a net flux of momentum in that direction as well.

The lowest order GWs in GR are quadrupolar. Recoil from GW emission must come (at lowest order) from a beating of the mass quadrupole with mass octupole and current quadrupole moments. The mass octupole and current quadrupole vanish for an equal mass binary, consistent with our "forward beaming" picture that unequal masses are needed for there to be any recoil. Thus GW recoil can be expected to be a very small effect, except perhaps in the very late stages of coalescence, since the octupole radiation amplitude is smaller than the quadrupole by a factor of order v/c (where v is orbital speed).

The first careful analysis of recoil in binary systems due to GW emission was by Michael Fitchett [127]. Fitchett's analysis described the orbital dynamics of the binary using Newtonian gravity and only included the lowest radiative multipoles which contribute to the recoil. His analysis predicted that the recoil of the merged remnant took the form

$$v_{\rm F} \simeq 1480\,{\rm km/sec}\frac{f(q)}{f_{\rm max}}\left(\frac{2G(m_1+m_2)/c^2}{R_{\rm term}}\right)^4 \,, \tag{1.58}$$

where $R_{\rm term}$ is the orbital separation at which GW emission terminates, $\mathrm{q} = m_1/m_2$ is the binary's mass ratio, and $\mathbf{f}(\mathrm{q}) = q^2(1-q)/(1+q)^5$ is a function whose maximum is at $\mathrm{q} \simeq 0.38$,

and has the limit $\mathbf{f}(q) \simeq q^2$ for $q \ll 1$.

Three features of this formula should be noted. First, this result does not depend on total mass but only on the mass **ratio** (recall $R_{\rm term}$ scales with total mass M). Thus, this scaling holds for any binary black hole merger — stellar mass mergers through supermassive mergers. Second, the overall scale is quite high. Although there is an important dependence on mass ratio and the termination radius $R_{\rm ,,,}$ is somewhat uncertain, Eq. (1.58) indicates that kicks of hundreds of km/sec are not difficult to achieve; kicks $\gtrsim$ 1000 km/sec are plausible. This is high enough that black hole ejection following a merger could to be common. Third, the recoil becomes very strong when the separation of the bodies is small. This is a strong hint that we cannot take **Eq.** (1.58) at face value — the strong gravity physics neglected by Ref. [127] is likely to be very important.

1.20.2 Astrophysical implication of gravitational wave recoil

The transport of linear momentum, the gravitational-radiation rocket effect, though a higher-order relativistic phenomenon, may have observable consequences on galactic scales. Radiation reaction from the coalescence of black holes from the cores of merging galaxies might, in a suitably asymmetric coalescence, eject the resulting black hole from the resulting galaxy. Thus the distribution of massive black holes in galaxy cores observed now could depend on the details of such highly dynamical black-hole interactions [128].

Observational consequences of kicks include: (i) the probability that BHs are ejected from galaxies and its implications for BH growth; (ii) the time scale for a kicked BH to return to the center of a galaxy, and (iii) the effect of displacement on nuclear structure [129].

In this thesis, we investigate the second post-Newtonian linear momentum flux for ICB moving in quasi-circular orbits. The 2PN linear momentum flux is then employed to first estimate the 2PN accurate GW recoil from the inspiral phase up to the ISCO. This calculation is then supplemented by the recoil arising from the plunge to the horizon from the ISCO.

1.21 Tests of general relativity using binary pulsar systems

The binary pulsar PSR 1913+16, discovered in 1974 by J. Taylor and R. Hulse, provided important new tests of general relativity: gravitational radiation and strong-field gravity. By timing of the pulsar "clock", important orbital parameters of the system could be measured with great precision. These included non-relativistic "Keplerian" parameters: eccentricity e, and orbital period P_b at any epoch; relativistic "post-Keplerian" parameters: the mean rate of advance of periastron, $\langle \dot{\omega} \rangle$, the effect of special relativistic time-dilation and the gravitational

redshift on the arrival time of pulses, (resulting from the pulsar's orbital motion and the gravitational potential of its companion), y', the rate of decrease of the orbital period (due to gravitational radiation damping, apart from a small correction due to galactic differential rotation). $\dot{P}_b$. Two other parameters, s and r, are related to the Shapiro time delay of the pulsar signal.

By combining the observations of PSR 1913+16 with the GR predictions, one obtains both a measurement of the two masses, and a test of GR, since the system is overdetermined. The results are [130]

$$m_1 = 1.4414 \pm 0.0002 M_\odot \quad , \quad m_2 = 1.3867 \pm 0.0002 M_\odot \, ,$$
$$\dot{P}_b^{\rm GR} / \dot{P}_b^{\rm OBS} = 1.0013 \pm 0.0021 \, . \tag{1.59}$$

The remarkable "double pulsar" J0737-3039 is a binary system with two detected pulsars, in a 0.10 day orbit seen almost edge on, with eccentricity $e = 0.09$, and a periastron advance of 17° per year. A variety of novel tests of relativity, neutron star structure, and pulsar magnetospheric physics will be possible in this system [131, 132]. For a review of binary pulsar tests, see [133].

1.21.1 Gravitational radiation tests of gravitational theory

The detection of gravitational radiation by either laser interferometers or resonant cryogenic bars will eventually lead to a new era of gravitational-wave astronomy [33, 134]. It will also yield new and interesting tests of general relativity (GR) in its radiative regime [135]. These relate to

1. *Polarization of gravitational waves:* General theories of gravity can have six independent states of polarizations. Three are transverse to the direction of propagation, with two representing quadrupolar deformations and one representing an axisymmetric "breathing" deformation. Three modes are longitudinal, with one an axially symmetric stretching mode in the propagation direction, and one quadrupolar mode in each of the two orthogonal planes containing the propagation direction. General relativity predicts only the first two transverse quadrupolar modes, while scalar-tensor gravitational waves can in addition contain the transverse breathing mode. A suitable array of gravitational antennas could measure the number of modes present in a given wave. If distinct evidence were found of any mode other than the two transverse quadrupolar modes of GR, the result would be a problem for GR.

2. *Speed of gravitational waves:* According to GR, GWs have the same speed, c, as light. In other theories, the speed could differ from c because of the coupling of gravitation to

"background gravitational fields. The speed of gravitational waves could also differ from c if gravitation were propagated by a massive field (a massive graviton), in which case v_g would be given in a local inertial frame by,

$$\frac{v_g}{c} = \left(1 - \frac{m_g^2 c^4}{E^2}\right)^{1/2} \approx 1 - \frac{1}{2}\frac{c^2}{f^2 \lambda_g^2}, \tag{1.60}$$

where m_g, E and f are the graviton rest mass, energy and frequency, respectively, and $\lambda_g = h/m_g c$ is the graviton Compton wavelength ($\lambda_g \gg c/\mathrm{f}$ assumed). The most obvious way to test for a massive graviton is to compare the arrival times of a gravitational wave and an electromagnetic wave from the same event, *e.g.* a supernova.

3. Radiation reaction: Bound on the graviton mass can also be set using gravitational radiation alone [136]. For an inspiralling compact binary as the frequency of the gravitational radiation sweeps from low frequency at the initial moment of observation to higher frequency at the final moment, the speed of the gravitational waves emitted will vary, from lower speeds initially to higher speeds (closer to c) at the end. This will cause a distortion of the observed phasing of the waves and result in a shorter than expected overall time At, of passage of a given number of cycles. Through the technique of matched filtering, the parameters of the compact binary can be measured accurately [137], and thereby the effective emission time At, can be determined accurately.

Finally, in this thesis we investigate the extent to which one can test general relativity using gravitational wave phasing in the ground-based GW interferometric detectors and more significantly space-based GW detector LISA.